RSC Advances

PAPER

View Article Online
View Journal | View Issue

Cite this: *RSC Adv.*, 2014, **4**, 20208

Boronate ester bond-based core–shell nanocarriers with pH response for anticancer drug delivery

Lei Sun, Xinge Zhang,* Jinxia An, Cui Su, Qianqain Guo and Chaoxing Li*

Currently, the major challenge for cancer treatment is to develop simple and smart nanocarriers that can efficiently retain the encapsulated drug during blood circulation, recognize tumor cells and quickly release the drug under stimulation. In this paper, such a pH-sensitive core–shell composite nanoparticles is prepared based on a 3-aminophenylboronic acid modified mesoporous silica nanoparticles (MSN–APBA) core coated with a lactobionic acid grafted chitosan (CS–LA) shell *via* boronate ester bonds. The MSN core increases drug loading capacity and stability, and lactobionic acid offers abundant diols which can form pH sensitive boronate ester bonds with APBA on MSN. Meanwhile, the lactobionic acid-conjugated shell could also efficiently target the asialoglycoprotein receptor over expressing hepatoma cells. The successful synthesis of CS–LA and MSN–APBA is confirmed by the results of TGA, TEM, DLS, FT-IR, ^{1}H-NMR and N_2 adsorption–desorption. Doxorubicin hydrochloride (DOX) is applied as a model drug and the behaviors of drug loading/release are investigated. The drug loading behavior is pH-dependent, and its drug encapsulation efficiency is near 80% and loading capacity is 13.05%. The results of cumulative *in vitro* release indicate that at neutral pH, the pores of the MSN are effectively capped with a polymer shell and the drug release is strongly inhibited, almost zero release. While at acidic pH, the hydrolysis of the boroester bond takes place and thus results in a rapid release of the entrapped drug. The cytotoxicity assay indicates high cell biocompatibility of this material and it is suitable as a drug carrier. When loaded with DOX, it presents distinctly cytotoxic behavior to HepG2 cells, due to the sustained release of drug. These results imply that the core–shell nanoparticles are promising platforms to construct simple and effective pH-responsive controlled drug delivery systems for cancer therapy.

Received 1st March 2014
Accepted 22nd April 2014

DOI: 10.1039/c4ra01812e

www.rsc.org/advances

1. Introduction

Within the last decade, achievements in the design of controlled drug delivery systems (DDSs) have led to an explosive development in the treatment of numerous diseases. These systems have been widely investigated and attracted increasing attention because they could offer many advantages, such as improved efficacy, reduced toxicity and side effects, reduced frequency of doses, and convenience.[1,2] Until now, various materials, such as dendrimers,[3] block polymers,[4] liposomes,[5] and many inorganic nano-materials have been utilized as drug carriers in DDSs. It is noteworthy that among them, the mesoporous silica nanoparticle (MSN) has been gained much importance due to its unique features, such as large surface area and pore volume, high chemical and thermal stability, excellent biocompatibility, and versatile chemistry for further functionalization.[6] Moreover, their small size as drug carriers allows them to overcome various biological barriers and achieve passive targeting through the enhanced permeability and retention (EPR) effect[7,8] which facilitates the delivery of drugs exclusively to the intended tissues without provoking adverse reactions in tumor therapy. However, conventional MSN are unintelligent materials with which drug release can not be accomplished in a precise control over the location. For instance, Vallet-Regi *et al.* had loaded ibuprofen into a series of MSN with different pore sizes and found that the release rate of drug decreased with the decrease of pore size.[9] However, in these systems, drug molecules were simply physically adsorbed in the channels of MSN and would be released immediately after administration, which would cause undesirable side effects to normal cells and organs. Lin *et al.* used CdS or Fe_3O_4 as a gate to demonstrate chemical reduction stimulated release from MSN in an aqueous environment.[10] Unfortunately, the potential use of these modified MSN was still limited because of the unwanted possible cytotoxicity of the unlinked nanoparticles gates. In order to tackle this issue, fabrication of stimuli-responsive polymer-coated MSN carriers is a useful strategy.[11]

Key Laboratory of Functional Polymer Materials of Ministry Education, Institute of Polymer Chemistry, Nankai University, Tianjin 300071, China. E-mail: zhangxinge@nankai.edu.cn; lcx@nankai.edu.cn; Fax: +86-22-23505598; Tel: +86-22-23501645

Typical biological stimuli exploited for favored drug release is pH which provides an efficient way to control the drug release behavior by pH stimuli. It could reduce the toxicity and side effects of drug for normal cells, and drug could be triggered released only in cancer cells. That was because most cancer tissues have lower extracellular pH values (pH 6.0–7.0) than normal tissues and the bloodstream (pH 7.4), and drops still further inside cells (4.5–5.5), especially.[12] Most reported MSN based pH sensitive materials have been made by three methods: (1) layer-by-layer adsorption technique, which is based on electrostatic attraction to assemble multilayered polyelectrolyte on the surface of MSN;[13] (2) "graft from" strategy, such as free radical polymerization and ATRP;[14] (3) "graft to" strategy, of which surface-initiated polymerizations initiated by functional groups on cores, such as –OH, $-NH_2$, $-CH{=}CH_2$, and –Br, *etc.*[15] Although some of them are successful, there are still some drawbacks, such as low encapsulation efficiency or difficulty to control the molecular weight of grafted polymers or the need of tedious processes to clean up the catalysts.[16] Therefore, it is still a challenge to explore a simple and facile method to prepare drug carriers that would be capable of recognizing the intrinsic pH differences between cancers and normal tissues and can present faster release behavior at low pH.

Chitosan (CS), a weak cationic polysaccharide produced by deacetylation of the natural polymer chitin, has many useful biological properties, such as biocompatibility, biodegradability, bioactivity and hydrophilicity as well as the possibility of coating particles with specific ligands. Herein, we proposed a facile and efficient strategy to synthesize pH-responsive nanocarriers with lactobionic acid grafted chitosan shells and APBA modified MSN cores. Lactobionic acid offers abundant diols which can form pH-sensitive boronate esters bond with APBA on MSN. What is more, lactobionic acid-conjugated shell could also efficiently target to asialoglycoprotein receptor over expressing hepatoma cells.[17] As shown in Scheme 1(B), at neutral pH, the linker remains intact and the entry of the pores on the MSN are blocked with polymer shell to strongly inhibit the molecular diffusion from the pores. At acidic pH (pH < 7.4), the shell was removed due to the hydrolysis of the boronate ester between APBA on MSN and diol on CS shell, allowing the release of the entrapped drug. Such well-designed core–shell composite nanocarriers had been engineered to respond to the slight difference of pH between tumor tissue and healthy tissue in the simulated physiological conditions. Doxorubicin hydrochloride (DOX), a well-known chemotherapeutic drug, was chosen as a model drug to assess the drug loading and releasing behaviors of core–shell nanoparticles. The *in vitro* cellular cytotoxicity test was performed to evaluate the biocompatibility of core–shell nanoparticles, and the cytotoxic effect of blank nanoparticles and DOX-loaded nanoparticles to cancer cells (HepG2) and embryo fibroblast cells (NIH3T3) were also investigated.

2. Experiment

2.1 Materials

Cetyltrimethylammonium bromide (CTAB) and tetraethoxysilane (TEOS) were purchased from Kemiou Chemical Co. Ltd.

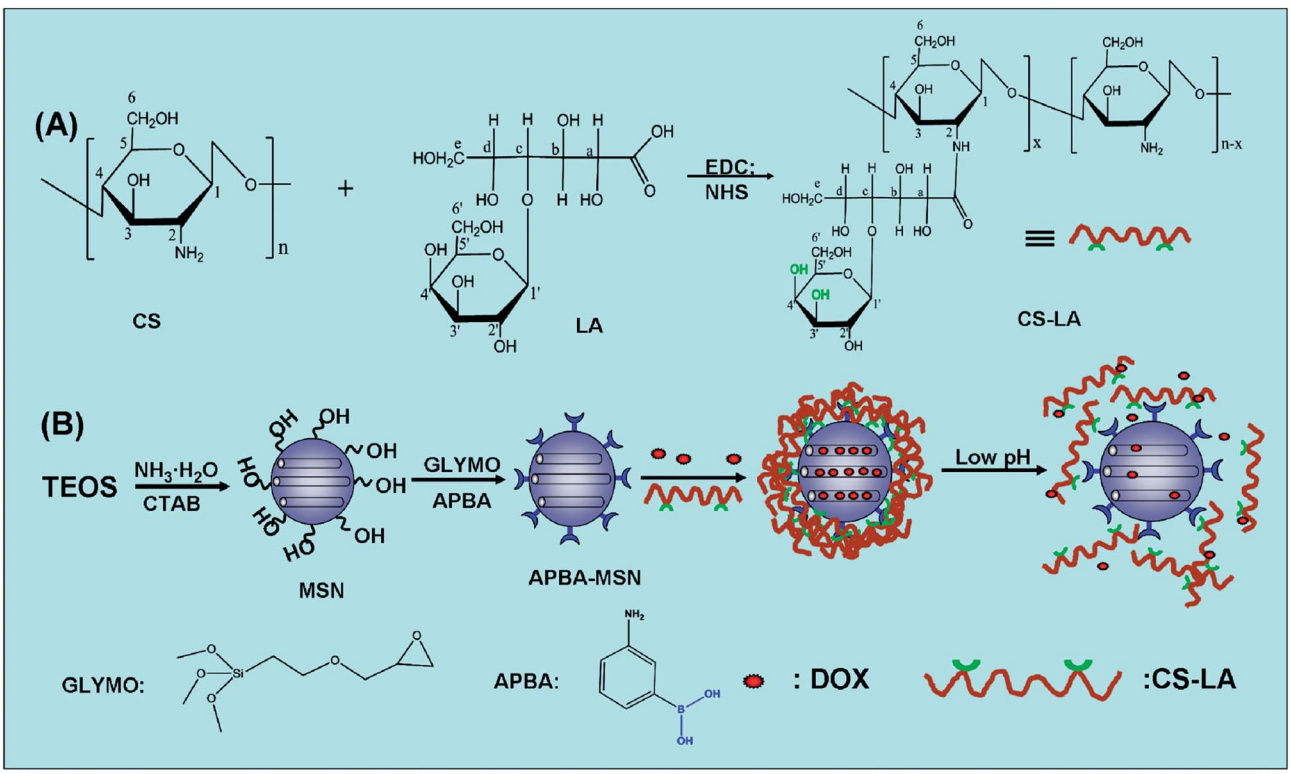

Scheme 1 (A) synthesis of CS–LA; (B) synthesis of MSN–APBA and experimental process for pH-controlled encapsulation and release of the model drugs DOX.

(Tianjin, China). 3-Glycidyloxypropyltrimethoxysilane (GLYMO, 98%), was available from aladdin (Beijing, China). 3-Amino phenylboronic acid monohydrate was purchased from Nanjing Kangmanlin Chemical Industry Co. Ltd. (Nanjing, China). Water soluble chitosan (molecule weight 50 kDa) were purchased from Yuhuan Ocean Biochemical Co. Ltd. (Zhejiang, China) and the degree of deacetylation was 93%. Lactobionic acid (LA), 1-ethyl-3-(3-dimethylaminopropyl)-carbodiimide hydrochloride (EDC) and *N*-hydroxysuccinimide (NHS) were available from aladdin (Beijing, China).

All other reagents were of analytical grade and were not further purified before used.

2.2 Synthesis of lactobionic acid grafted chitosan (CS–LA)

Coupling of lactobionic acid with the chitosan was performed using EDC and NHS as coupling agents.[18,19] Briefly, 358 mg of LA dissolved in 10 mL of distilled water was activated with a mixture of NHS (115 mg) and EDC (310 mg). Subsequently, 80 mg of chitosan was dissolved in 5 mL of 1% HCl (vol/vol) solution and then added into the LA solution (Scheme. 1(A)). The reaction was performed for 72 h at room temperature. The resulting product was purified using a dialysis tube (12 000 MWCO) against distilled water for 3 days; a light-yellow powder was obtained followed by lyophilization. The chemical structure of CS–LA was confirmed through FT-IR and ^{1}H-NMR. The degree of substitution (DS) of galactose residues in CS–LA estimated by 1H-NMR was calculated as follows: DS = $[H_{CS-LA(\delta 3.41-4.15)} - H_{CS(\delta 3.38-3.91)}/12] \times 100\%$ where $H_{CS-LA(\delta 3.41-4.15)}$ was the number of hydrogen atoms of CS–LA at δ3.41–4.15, and $H_{CS(\delta 3.38-3.91)}$ was the number of hydrogen atoms of CS at δ3.38–3.91.

2.3 Synthesis of 3-aminophenylboronic acid modified mesoporous silica nanoparticles (MSN–APBA)

3-aminophenylboronic acid modified mesoporous silica nanoparticles (MSN–APBA) were synthesized by two steps. Firstly, 3-glycidyloxypropyltrimethoxysilane modified MSN (GLYMO–MSN) were obtained by a typical CATB-templated, base-catalyzed sol–gel method.[20] Briefly, 0.08 g of CTAB was dissolved in 40 mL of H_2O, and 0.5 mL of $NH_3 \cdot H_2O$ (30%) was added with stirring for 0.5 h. A 0.2 mL portion of TEOS was then added with vigorous stirring for 6 h at room temperature. Then, excess GLYMO (0.1 mL) was added to the above MSN under stirring and the mixture was stirred for another 4 h at room temperature. Secondly, APBA 25 mg was dissolved with 2 mL of ethanol, and then dropped slowly into GLYMO–MSN solution, kept stirring for 3 h.[21] The resultant nanoparticles containing template were collected by centrifugation, and washed with distilled water/ethanol. The templates inside the MSN–APBA were removed by ion-exchange with NH_4NO_3/C_2H_5OH: 0.5 g of MSN–APBA powder was dispersed in 50 mL of ethanol containing 0.3 g of NH_4NO_3, refluxed twice at 60 °C for 4 h, centrifuged, washed three times with distilled water and ethanol, and then dried in a vacuum.

2.4 Characterization of nanoparticles

The FT-IR spectra of samples were recorded in KBr pellets in a Fourier transform infrared spectrometer (Bio-Rad FTS-6000) in the range of 4000–300 cm^{-1} for 32 scans. The morphology of MSN–APBA and the resultant core–shell nanoparticles were determined by transmission electron microscopy (TEM). Samples for TEM characterization were dispersed in solvent and a drop of the dispersion was spread onto the surface of a copper grid coated with a carbon membrane and then dried in vacuum at room temperature for characterization. The hydrodynamic diameter of MSN–APBA was determined by dynamic light scattering (DLS) using a laser light scattering spectrometer (BI-200SM) equipped with a digital correlator (BI-9000AT). All samples were prepared from the suspension with a concentration of 10 μg mL^{-1} after ultrasonic dispersion and measured at different pH values, respectively. The thermo-gravimetric analysis of the nanoparticles, using 10 mg per sample, was conducted in nitrogen, at a heating rate of 10 °C min^{-1}, using a thermo-gravimetric analyzer (TGA; TG 209, NETZSCH). Real compositions of shells were tested by Element analysis (vario EL CUBE). N_2 sorption analysis was performed on an ASAP 2020/Tristar 3000 volumetric adsorption analyzer at 77 K.

2.5 Encapsulation efficiency (EE) and loading capacity (LC) of anti-cancer drug doxorubicin (DOX)

To evaluate the drug loading capacity and release properties, DOX was used as a model anticancer agent. To entrap the free DOX into MSN–APBA, DOX (2.5 mg) was added to 5 mL of the PBS buffer solution (pH 7.4, 6.1, 4.9) containing MSN–APBA (5.0 mg) and the mixture was stirred for 24 h. Subsequently, 10 mg of CS–LA was added to form core–shell structure, thus, DOX could be blocked in mesoporous cores. Then the drug-loaded nanoparticles were separated by centrifugation. The concentration of the remaining DOX solution was determined by a fluorescence spectrophotometer using an excitation of 485 nm. A standard plot was prepared under identical conditions to confirm the amount of drug loaded by the nanocomposites. The EE and LC of DOX were calculated as follows:[22,23]

$$\mathrm{EE}\% = \frac{\text{total DOX} - \text{free DOX}}{\text{total DOX}} \times 100\%$$

$$\mathrm{LC}\% = \frac{\text{total DOX} - \text{free DOX}}{\text{nanoparticles' weight}} \times 100\%$$

All measurements were performed in triplicate and averaged.

2.6 *In vitro* release from core–shell nanoparticles

DOX release from core–shell nanoparticles was analyzed by incubating the nanoparticles in PBS with different pH values (pH = 4.9, 6.1 and 7.4) at 37 °C while shaking. At predetermined time-points, samples were centrifuged at 10 000 rpm for 5 min (KDC-160-HR; 4 °C, angle rotor: 1#) and the supernatant was taken and replenished by fresh PBS. The amount of free DOX

was determined by a fluorescence spectrophotometer using an excitation of 485 nm and a calibration curve was generated using blank nanoparticles to correct for the intrinsic absorption of the polymer. In each experiment, the samples were analyzed in triplicate with error bars representing the standard deviation.

2.7 Analysis of *in vitro* release

To determine the DOX release mechanism, the amount of DOX released *versus* time was studied using the following mathematical model:

$$M_t/M_\infty = kt^n$$

where M_t/M_∞ is the fractional amount of the DOX released at time t, k is a characteristic constant, and n is the release exponent, depending on the release mechanism and the geometry of the device. From the slope and intercept of the plot of $\log(M_t/M_\infty)$ *vs.* $\log t$, kinetic parameters n and k were calculated. If Fickian diffusion occurs, n lows 0.5 for slab/cylinder/sphere. If non-Fickian (anomalous) diffusion dominates, the n value is between the above value corresponding to the polymer chain relaxation ($n < 1$) for slab/cylinder/sphere. So through determination of n value, the DOX release mechanism was identified.[24]

2.8 *In vitro* cytotoxicity

MTT method was used as an assay for assessing the effects of drug carriers in various concentrations. In brief, well-growing HepG2 cancer cells and NIH3T3 cells were placed in 96-well plates (5000 cells per well) and five duplicate wells were set up in each sample. The culture medium was replaced with the medium containing different concentrations of nanoparticles without and with DOX (125, 250, 500 μg mL^{-1}) and cultured at 37 °C in a humidified atmosphere (5% CO_2/95% O_2) with the cells anchored to the plates for 48 h. Each sample was tested in three replicates per plate. After incubation, 10 μL of MTT (1 mg mL^{-1}) solutions was added in each well. The plates were then returned to the incubator and incubated for a further 4 h in 5% CO_2 at 37 °C. Then, the culture medium and MTT were removed. DMSO (0.1 mL) was then added to each well to dissolve the formazane crystals. The optical density was read on a microplate reader at 490 nm. Cell viability was determined as a percentage of the negative control (untreated cells).[25] One-way analyses of variance was followed by multiple comparisons with Student Newman–Keul's tests and $p < 0.05$ was regarded as significant.

3. Result and discussion

3.1 Synthesis of CS–LA

CS–LA was prepared by the similar method previously reported.[17,18] The synthesis was shown in Scheme 1.

FT-IR spectra of CS, LA, and CS–LA was shown in Fig. 1(A). We found that CS exhibited characteristic absorptions at 1662 and 1590 cm^{-1}, which were attributed to amides I and II, respectively.[26] The IR spectrum of LA exhibited a broad –OH

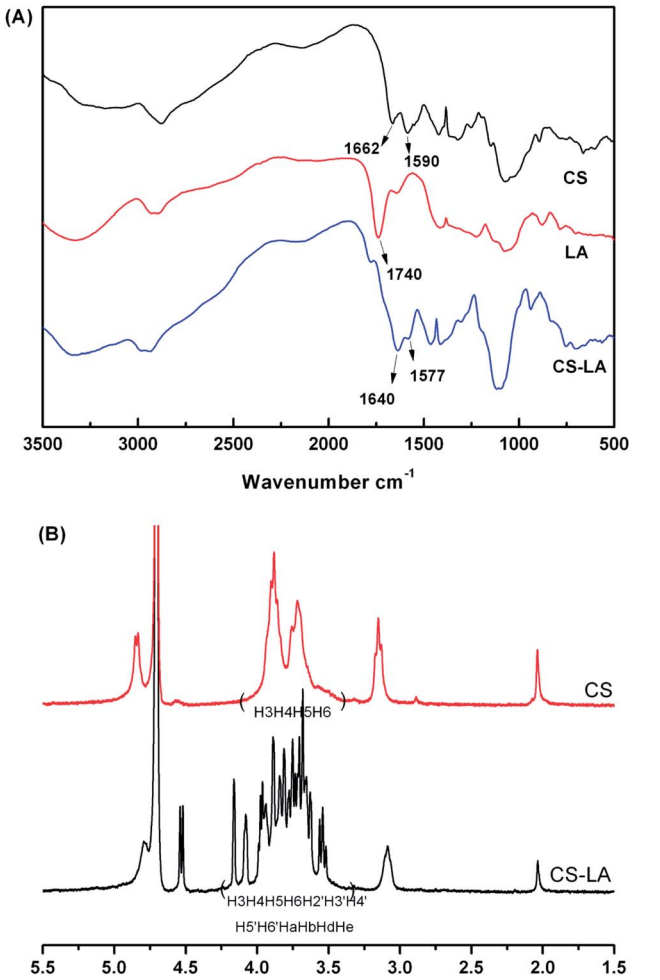

Fig. 1 (A) The FT-IR spectra of CS, LA and CS–LA; (B) the ^{1}H-NMR spectra of CS and CS–LA.

absorption occurring in the region between 3400 and 2400 cm^{-1}, and a distinctive band at 1740 cm^{-1} due to the carbonyl stretching (C═O) of carboxylic groups. In the IR spectrum of CS–LA, the carbonyl stretching of LA disappeared due to the amide bond formation between carboxylic groups of LA and amine groups of CS. All peaks of amides I and II of GC slightly shifted from 1662 and 1590 to 1640 and 1577 cm^{-1}, respectively, when compared with those of CS, an indication of the conformational change of CS after reaction with LA. Furthermore, the O–H stretching peak of GC, which appeared at around 3450 cm^{-1}, shifted to a higher wave number, which indicated that the intermolecular hydrogen bonding between CS–LA chains increased due to the introduction of LA to the CS chains.[27]

Fig. 1(B) shows ^{1}H-NMR spectra of CS and CS–LA (D_2O/F_3CCOOD, 400 MHz). CS, δ (ppm): 4.57 (H_1), 3.09 (H_2), 3.38–3.91 (H_3, H_4, H_5, H_6); CS–LA, δ (ppm): 4.59(H_1), 3.41–4.15 (H_3, H_4, H_5, H_6, $H_{2'}$, $H_{3'}$, $H_{4'}$, $H_{5'}$, $H_{6'}$, Ha, Hb, Hd, He), the substitution value of LA in CS–LA was calculated by comparing the characteristic peak areas of LA group (4.1 ppm) with that of 2.0 ppm peak attributed to the original acetamide group of chitosan. The substitution values of LA coupled with chitosan in GC was estimated by 12.8 mol%.

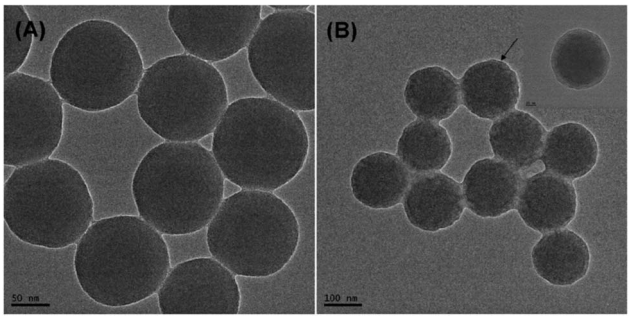

Fig. 2 TEM images of (A) MSN–APBA; (B) MSN–APBA coated with CS–LA.

3.2 Synthesis of MSN–APBA

Procedure for the synthesis of MSN–APBA was shown in Scheme 1(B). Monodisperse MSN–APBA with an average size of 140 nm was synthesized *via* the modified Stöber method. The morphology of the MSN–APBA was observed by TEM, as shown in Fig. 2(A). MSN–APBA nanoparticles had a spherical shape with an average diameter of 140 nm and a good monodispersity. After coated with CS–LA, the MSN–APBA presented a uniform core–shell structure which was shown in Fig. 2(B).

Further, in order to define the particle size and stability, we also measured their size by DLS and their zeta potential as shown in Table 1. Their diameters were 145.2, 147.1 and 146.7 nm under pH 4.9, 6.1 and 7.4, respectively, which was consistent from the data obtained by TEM. Their zeta potential decreased from 23.5 to 12.1 as pH increased from 4.9 to 7.4, for the reason that APBA mostly existed with its negative charged form at relative high pH.

From the FT-IR spectra of MSN–APBA(Fig. 3(A)), a strong peak at 1082.8 cm^{-1} and medium-sized peaks at 790.2 and 948.1 cm^{-1} corresponding to the symmetrical and asymmetrical vibrations of the Si–O–Si bond and the stretching vibration of the hydroxyl group, respectively. Moreover, the existence of bands at 1384.0, 710.3 cm^{-1} due to vibrations of B–O bonds clearly suggests that boronic-acid-functionalized silica material is obtained. After coated with CS–LA, the core–shell nanoparticles presented characteristic peaks of amides near 1600 cm^{-1} compared with the FT-IR spectra of CS–LA (Fig. 1), furthermore, the O–H stretching peak, appeared at around 3450 cm^{-1}, shifted to a higher wavenumber compared with MSN–APBA, which also indicated the successful introduction of CS–LA onto the MSN–APBA. Inorder to identify it pH sensitivity, we treated the core shell nanoparticles with acid (pH 4.9), and then

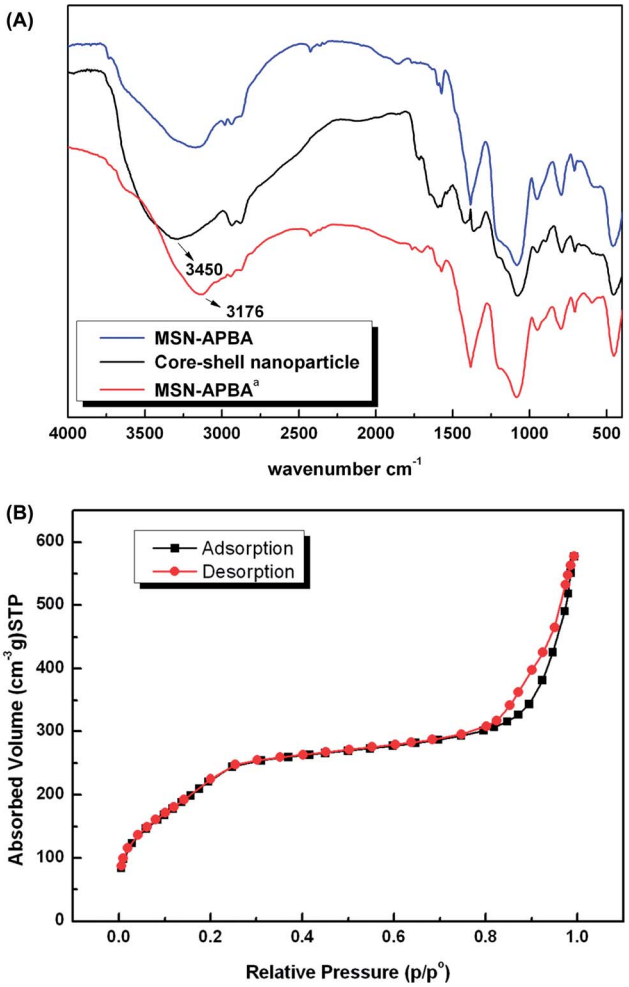

Fig. 3 (A) The FT-IR spectra and (B) nitrogen adsorption–desorption isotherm of MSN–APBA.

centrifugated, dried till constant weight, its FT-IR (Fig. 3(A) MSN–APBA[a]) confirmed that the O–H stretching peak shifted back to lower wavenumber of 3176 cm^{-1} almost the same with MSN–APBA, indicated the disappearance of CS–LA due to the hydrolysis of the boroester bond between CS–LA and MSN–APBA.

Further, the porosity of the MSN–APBA was studied by measuring the nitrogen adsorption–desorption isotherm and BET surface area. Fig. 3(B) depicted the N_2 adsorption–desorption isotherm. The BET specific surface area was calculated to be 862.15 $m^2\ g^{-1}$. The isotherm could be classified as type IV with an apparent hysteresis loop in the range of 0.5–1.0P/P_0

Table 1 Sizes and zeta potentials under different pH values

	pH 4.9		pH 6.1		pH 7.4	
	D_n[a]	Zeta	D_n[a]	Zeta	D_n[a]	Zeta
MSN–APBA	145.2 ± 2.3	23.5 ± 3.2	147.1 ± 3.1	18.3 ± 2.4	146.7 ± 4.8	12.1 ± 4.1

[a] D_n was obtained by DLS.

indicating the presence of mesoporous structure in the MSN–APBA. The average pore size calculated from the adsorption branch of the nitrogen isotherms by the Barrett–Joyner–Halenda (BJH) method was 3.7 nm. The presence of pores provided the repository for DOX loading.

3.3 Loading and release *in vitro*

DOX was used as a model drug to investigate the potential application of the pH-sensitive composite nanoparticles. This kind of nanoparticles was loaded with DOX (2 : 1 w/w) at various pH. The LC and EE were measured by UV and TGA method. It was evident from Table 2 that the amount of loading was significantly affected by pH. When pH increased from 4.9 to 7.4, the LC increased from 4.67% to 13.05% and EE increased from 28.07% to 78.31% (Table 2). Accordingly, Fig. 4(A) indicated that nanoparticles without DOX and with DOX loading under different pH presented weight loss from 47.48% to 59.88%. The DOX loading process was predominantly based on the physical adsorption mechanism and electrostatic interactions in mesoporous channels. As pH increased,[28] the net charge of DOX was around zero thus the electrostatic interactions between the polymer shell and drug molecules were minimal[29] while DOX molecules would easily absorbed into the mesoporous pores with the elevated pH values.

Table 2 DOX loading capacity (LC) and encapsulation efficiency (EE) under different pH values

pH	EE (%)	LC (%)
7.4	78.31 ± 3.04	13.05 ± 0.21
6.1	39.21 ± 2.54	6.53 ± 1.05
4.9	28.07 ± 2.03	4.67 ± 2.12

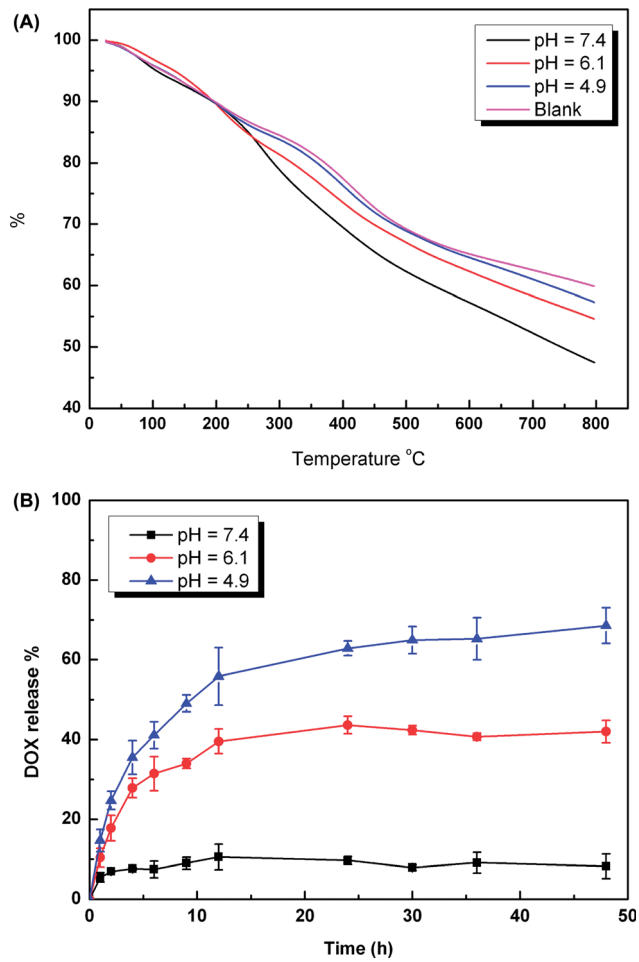

Fig. 4 (A) Thermal analysis of DOX loaded under different pH and blank nanoparticles; (B) release profiles of DOX from core–shell nanoparticles in the solution with different pH values.

The next investigation was to demonstrate whether core–shell nanoparticles showed a pH-sensitive release of DOX. The drug release was conducted in the simulated body fluids and the release data at pH 7.4, 6.1 and 4.9 were shown in Fig. 4(B). While at pH 7.4, only 8.5% of DOX was released after 48 h, and there was almost no initial burst release in the system. With the decrease of pH in the solution, DOX release from core–shell nanoparticles in the acidic conditions (pH 6.1 and 4.9) showed a relatively rapid rate. After 48 h, the amount of released DOX reached 38.8% at pH 6.1 and 68.8% at pH 4.9, respectively. We supposed that there were two reasons for that. As we mentioned above, the interaction between diols on the shell and APBA on the core become weaker while pH decreased, leading to the detachment of shell, thus, the blocked pores came into open and DOX released rapidly. On the other hand, at low pH, the enhanced electrostatic repulsion between the positively charged drug molecules and the positively charged mesoporous cores was favorable for the rapid release of DOX molecules. The pH-dependent release behavior from core–shell nanoparticles was of great interest in achieving tumor-targeted drug delivery. It was expected that DOX was sufficiently stable in the core–shell nanoparticles with minimal drug leakage during circulation in the blood. Then, upon reaching the targeted tumor tissues, by the effect of low pH and EPR, the rapid release of DOX from the core–shell nanoparticles would be subject to a certain increase.

In order to explore the release mechanism, the release data was analyzed according to the Ritger–Peppas equation.[24] The results show that R^2 was higher than 0.85 and n was lower than 0.5 in all cases (Table 3), indicating that DOX release was controlled by a drug diffusion process. Such system would allow the improvement of the drug release and a total accumulation in tumor tissues.

Table 3 DOX release kinetic data obtained from *in vitro* release experiments

	Ridger–Peppas model			
pH	n	k_1	R^2	Transport mechanism
7.4	0.20	0.06	0.86	Diffusion controlled
6.1	0.40	0.09	0.88	Diffusion controlled
4.9	0.42	0.13	0.93	Diffusion controlled

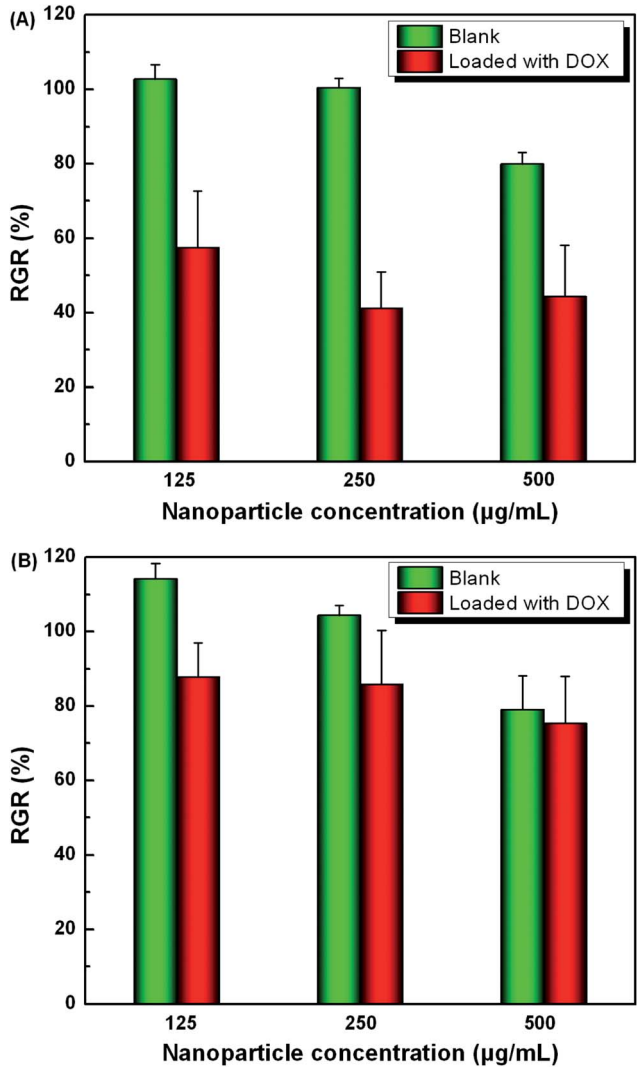

Fig. 5 Relative cell viabilities of HepG2 (A) and NIH 3T3 (B) cells incubated with different concentrations of core–shell nanoparticles (blank) and nanoparticles loaded with DOX.

3.4 *In vitro* cell assay

To evaluate core–shell nanocarriers being potentially applied as effective drug carrier for target treatment of tumors, *in vitro* cytotoxicity against HepG2 cancer cells (Fig. 5(A)) and NIH 3T3 cells (Fig. 5(B)) were investigated by MTT assay, respectively. As shown in Fig. 5, the blank carrier of nanoparticles displayed almost no obvious cytotoxitity on the HepG2 and NIH 3T3 cells even at a concentration of 500 μg mL^{-1}. Significant growth inhibition of HepG2 cells was observed when the cells were treated with the suspension of DOX-loaded core–shell nanoparticles. Over 60% of the cells presented growth inhibition after incubation with DOX-loaded core–shell nanoparticles. Furthermore, incubation of core–shell nanoparticles with and without DOX under different concentrations resulted in almost no cytotoxicity to NIH 3T3 cells. That was to say, lactobionic acid grafted chitosan exhibits high specificity to asialoglycoprotein receptor (ASGP-R)-overexpressing HepG2 cells[30] and the relatively low pH condition around HepG2 cells trigged the fast release of DOX. The results show that it was a non-toxic material even at the relatively high concentration and was suitable as a drug carrier. Compared to the resultant data, the cell viability of HepG2 show a significant difference compared with that of NIH 3T3 ($p < 0.05$). As anticipated, the core–shell nanoparticles were intriguing candidates for effective targeting drug carriers in the tumor therapy.

4. Conclusion

In this study, a kind of pH-sensitive core–shell composite nanocarrier was prepared based on APBA modified MSN core coated with lactobionic acid-grafted chitosan shell *via* the boronate ester linker. The DOX loading behavior of the composite microsphere was pH-dependent, and the composite microsphere had a maximal EE of about 80% at neutral pH. The cumulative *in vitro* release showed a low leakage of only 8.5% at pH 7.4 within 48 h but was significantly enhanced to 68.8% at pH 4.9, indicating that the drug release was apparently pH responsive. Moreover, the blank carrier showed no cytotoxicity to both NIH 3T3 and HepG2 cells at high concentrations of 500 μg mL^{-1}. However, significant growth inhibition of HepG2 cells was observed when the cells were treated with DOX-loaded nanoparticles. Therefore, this investigation demonstrated that pH-sensitive composite nanoparticles had the potential to overcome the lack of selectivity of anti-cancer drugs. Overall, the simple and efficient nature of the approach, coupled with the capability to achieve good therapeutic efficacy, made the prepared pH sensitive nanoparticles a promising site specific anticancer drug delivery carrier.

Acknowledgements

This work was supported by the National Natural Science Foundation of China (Grant no. 81170773) and PCSIRT (IRT 1257).

References

1 Z. Yan, R. Bao, Y. Huang, A. N. Caruso, S. B. Qadri, C. Z. Dinu and D. B. Chrisey, *J. Phys. Chem. C*, 2010, **114**, 3869–3873.
2 S. Kapoor and A. J. Bhattacharyya, *J. Phys. Chem. C*, 2009, **113**, 7155–7163.
3 L. Liu, B. Chen and F. Teng, *Int. J. Nanomed.*, 2010, **5**, 109.
4 X. Yang, J. J. Grailer, I. J. Rowland, A. Javadi, S. A. Hurley, V. Z. Matson and S. Gong, *ACS Nano*, 2010, **4**, 6805–6817.
5 L. Hosta-Rigau, R. Chandrawati, E. Saveriades, P. D. Odermatt, A. Postma, F. Ercole and F. Caruso, *Biomacromolecules*, 2010, **11**, 3548–3555.
6 J. T. Sun, C. Y. Hong and C. Y. Pan, *J. Phys. Chem. C*, 2010, **114**, 1248112486.
7 J. Dobson, *J. Mater. Chem.*, 2009, **19**, 6294–6307.
8 K. Riehemann, S. W. Schneider, T. A. Luger, B. Godin, M. Ferrari and H. Fuchs, *Angew. Chem., Int. Ed.*, 2009, **121**, 886–913.
9 M. Vallet-Regi, A. Ramila, R. P. Del Real and J. Perez-Pariente, *Chem. Mater.*, 2001, **13**, 308–311.

10 C. Y. Lai, B. G. Trewyn, D. M. Jeftinija, K. Jeftinija, S. Xu, S. Jeftinija and V. S. Y. Lin, *J. Am. Chem. Soc.*, 2003, **125**, 4451–4459.
11 B. S. Chang, X. Y. Sha, J. Guo, Y. F. Jiao, C. C. Wang and W. L. Yang, *J. Mater. Chem.*, 2011, **21**, 9239–9247.
12 D. Schmaljohann, *Adv. Drug Delivery Rev.*, 2006, **58**, 1655–1670.
13 Y. Wang, A. Yu and F. Caruso, *Angew. Chem., Int. Ed.*, 2005, **44**, 2888–2892.
14 F. Carniato, C. Bisio, G. Paul, G. Gatti, L. Bertinetti, S. Coluccia and L. Marchese, *J. Mater. Chem.*, 2010, **20**, 5504–5509.
15 R. Liu, P. Liao, J. Liu and P. Feng, *Langmuir*, 2001, **27**, 3095–3099.
16 K. Miyasaka, A. V. Neimark and O. Terasaki, *J. Phys. Chem. C*, 2008, **113**, 791–794.
17 R. Yang, F. H. Meng, S. B. Ma, F. S. Huang, H. Y. Liu and Z. Y. Zhong, *Biomacromolecules*, 2011, **12**, 3047–3055.
18 I. K. Park, J. Yang, H. J. Jeong, H. S. Bom, I. Harada, T. Akaike and C. S. Cho, *Biomaterials*, 2003, **24**, 2331–2337.
19 T. W. Chung, J. Yang, T. Akaike, K. Y. Cho, J. W. Nah, S. I. Kim and C. S. Cho, *Biomaterials*, 2002, **23**, 2827–2834.
20 R. I. Nooney, D. Thirunavukkarasu, Y. Chen, R. Josephs and A. E. Ostafin, *Chem. Mater.*, 2002, **14**, 4721–4728.
21 Y. W. Xu, Z. X. Wu, L. J. Zhang, H. J. Lu, P. Y. Yang and A. Paul, *Anal. Chem.*, 2009, **81**, 503–508.
22 W. Chen, F. H. Meng, F. Li, S. J. Ji and Z. Y. Zhong, *Biomacromolecules*, 2009, **10**, 1727–1735.
23 Y. F. Zhu, Y. Fang, L. Borchardt and S. Kaskel, *Microporous Mesoporous Mater.*, 2011, **141**, 199–206.
24 A. Nikolaos, *Pharm. Acta Helv.*, 1985, **60**, 110–111.
25 O. J. Kwon, D. J. Siegwart, H. I. Lee, G. Sherwood, L. Peteanu and J. O. Hollinger, *J. Am. Chem. Soc.*, 2007, **129**, 5939–5945.
26 C. Peniche, W. Arguelles-Monal, N. Davidenko, R. Sastre, A. Gallaredo and J. S. Roman, *Biomaterials*, 1999, **20**, 1869–1878.
27 H. Ali and T. S. Riahi, *Carbohydr. Res.*, 1983, **122**, 241–248.
28 A. Choucair, S. P. Lim and A. Eisenberg, *Langmuir*, 2005, **21**, 9308–9313.
29 Y. Wang, A. D. Price and F. Caruso, *J. Mater. Chem.*, 2009, **19**, 6451–6464.
30 B. Saunier, M. Triyatni, L. Ulianich, P. Maruvada, P. Yen and L. D. Kohn, *J. Virol.*, 2003, **77**, 546–559.